

Petrology and origin of the Lar igneous complex of the Sistan suture zone, Iran

Mohammad Boomeri, Rahele Moradi*, Sasan Bagheri

Department of Geology, Faculty of Sciences, University of Sistan and Baluchestan, Zahedan, Iran

*corresponding author: rmoradi@pgs.usb.ac.ir

Abstract

The Oligocene Lar igneous complex is located in the Sistan suture zone of Iran, being emplaced in Paleocene to Eocene flysch-type rocks. This complex includes mainly intermediate K-rich volcanic (trachyte, latite and andesite) and plutonic (syenite and monzonite) rocks that belong to shoshonitic magma. The geochemical characteristics of the Lar igneous complex, such as an enrichment of LREE and LILE relative to HREE and HFSE, respectively, a negative anomaly of Ti, Ba and Nb and a positive anomaly of Rb and Th are similar to those of arc-type igneous rocks. Tectonic discrimination diagrams also show that rocks of the Lar igneous complex fall within the arc-related and post-collisional fields and K-enrichment of these rocks confirm the post-collisional setting. Based on geochemical features, the Lar igneous complex magma was derived from partial melting of a phlogopite-bearing, enriched and metasomatised lithospheric mantle source and the magma was affected by some evolutionary processes like fractional crystallisation and crustal contamination.

Key words: Post-collisional setting, shoshonitic magmatism, rock properties, Middle East

1. Introduction

The Lar igneous complex is a unique example of potassic igneous rocks with different textures and unusual compositions that are associated with Cu-Mo mineralisation. The geology, geochemistry and petrology of this complex have been the subject of a few studies (Chance, 1981; Camp & Griffis, 1982; Tirrul et al., 1983; Bagheri & Bakhshi, 2001; Ghafari-Bijar, 2009; Farokh-Nezhad, 2011; Soltanian, 2013). According to Chance (1981) the Lar igneous complex is a late Oligocene, low-Ti post-tectonic igneous complex with features of a collapsed caldera. Camp & Griffis (1982) defined it as a late Oligocene alkaline volcanic-plutonic complex, while Bagheri & Bakhshi (2001) thought that it was an igneous ring dyke complex that formed as a result of caldera collapse, in relation to shoshonitic lamprophyric magmatism.

Despite previous studies, information on the geochemistry and petrology of the Lar igneous complex was not presented and our knowledge of the geology and geochemistry of this complex is still very poor. The Lar igneous complex consists of a wide variety of basic, intermediate and felsic rocks, but intermediate rocks predominate in this complex. Therefore, the present paper focuses on the petrological and geochemical characteristics of intermediate igneous rocks of the Lar igneous complex. We use whole-rock geochemistry of these rocks to discuss these geochemical characteristics, tectonic setting and petrogenesis.

2. Geological setting

The Lar igneous complex is located 20 km north-east of the city of Zahedan in the Sistan suture zone,

southeastern Iran (Fig. 1A, B). Iran has a complex geology with several tectono-stratigraphical zones (Fig. 1B). The Sistan suture zone is known as a remnant of a Cretaceous oceanic basin that extends as a N-S trending belt over more than 700 km (Tirrul et al., 1983). This zone is located between the Lut block in the west and the Afghan block in the east. The Sistan suture zone was divided into the Neh and Ratuk accretionary prisms and the Sefidabeh forearc basin (Camp and Griffis, 1982).

The Neh and Ratuk accretionary prisms are characterised by strongly deformed and faulted masses of ophiolite-melange, Upper Cretaceous to Eocene phyllite and Paleogene terrigenous-marine sedimentary rocks. In contrast, the Sefidabeh forearc basin contains a minor ophiolite-melange and has a coherent stratigraphy. Based on Camp & Griffis (1982) and Tirrul et al. (1983), the Sistan su-

ture zone is characterised by the following features: (A) the Upper Cretaceous ophiolite-melange masses (the oldest igneous rocks in this area) occur in all parts of the Sistan suture zone, especially in the western part, and are composed of ultramafic, mafic and sedimentary rocks; (B) flysch-type rocks, the most dominant and thickest rocks in the Sistan suture zone, unconformably cover the ophiolite-melange masses, and (C) non-ophiolitic igneous rocks that are different in age, composition and genesis and can be divided on the basis of age as follows: (1) Eocene calc-alkaline rocks that are attributed to the subduction of the Lut block beneath the Afghan block (Camp & Griffis, 1982). (2) Eocene to lower Oligocene Zahedan calc-alkaline I, rare S- and hybrid-type granitoids that are related to subduction and collision events in the area (Camp & Griffis, 1982; Boomeri et al., 2005; Sadeghian et al., 2005;

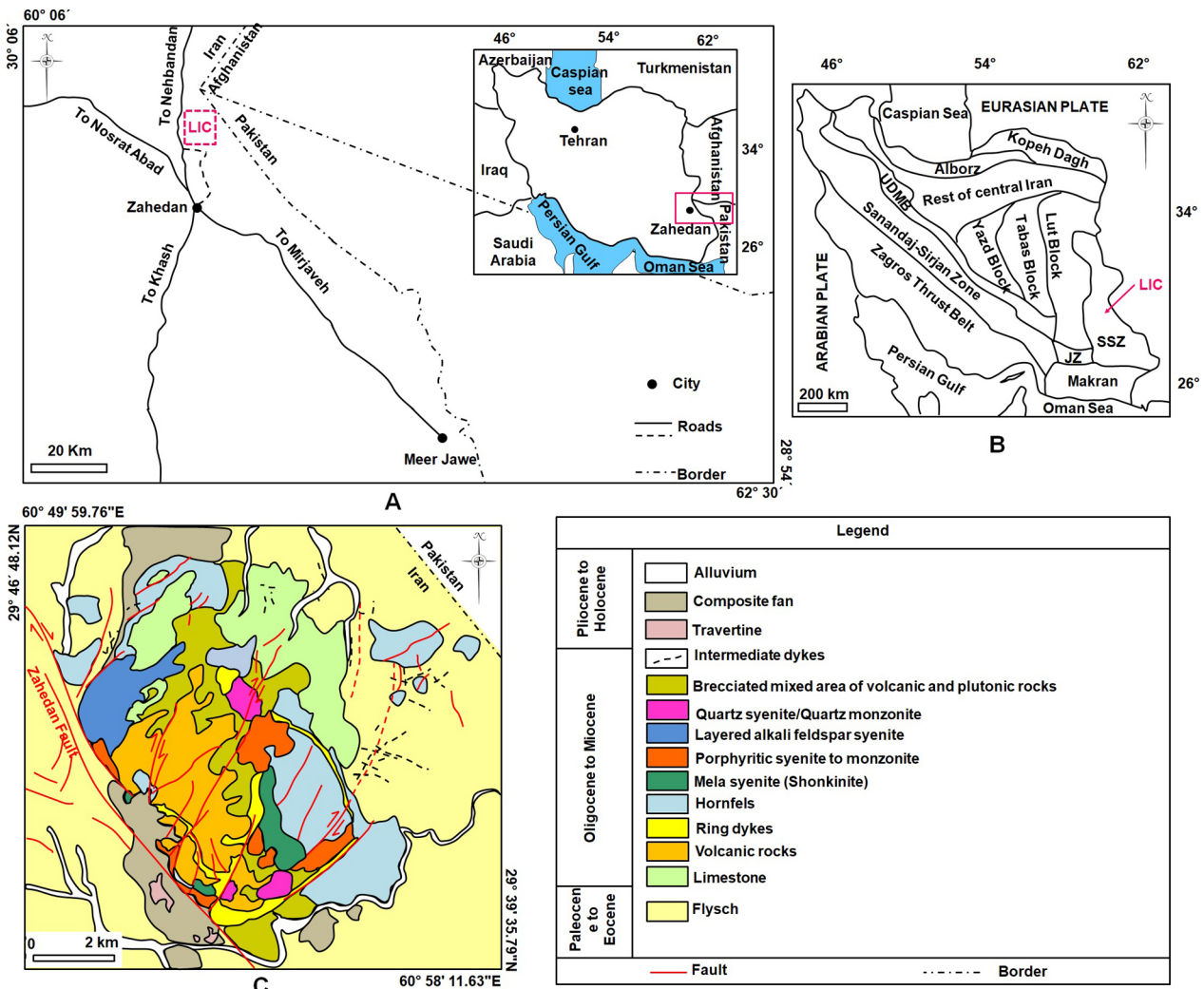


Fig. 1. A - Lar igneous complex location in the Sistan and Baluchestan province; B - Main tectono-stratigraphical units of Iran (Stöcklin, 1968); C - Geological units of the Lar igneous complex. UDMB = Urumieh-Dokhtar Magmatic Belt; JZ = Jazmorian; SSZ = Sistan Suture Zone

Sadeghian & Valizadeh, 2007; Rahnama-Rad et al., 2008; Ghasemi et al., 2010; Moradi et al., 2014; Mohammadi et al., 2016). (3) Oligocene to middle Miocene alkaline and calc-alkaline igneous rocks (shoshonite) such as the Lar igneous complex (Camp & Griffis, 1982). The alkaline and high-K calc-alkaline (shoshonitic) magmatism is closely related to major transcurrent faults in the eastern part. These faults are important post-collisional structural features in the Sistan suture zone (Camp & Griffis, 1982; Walker & Jackson, 2004). (4) Quaternary volcanic rocks like Mount Taftan that are related to the Makran active subduction of the Arabian Plate under the Makran accretionary prism and the Sistan suture zone (Farhoudi & Karig, 1977).

The Lar igneous complex is elliptical in shape and hosted by Upper Cretaceous, Paleocene and Eocene flysch-type rocks such as siliceous shale, sandstone, siltstone and minor limestone (Fig. 1C). Its longer dimension parallels the Zahedan fault system in the western and southwestern parts (Fig. 1C). Near the contact, the hosted sedimentary rocks were metamorphosed into hornfels and skarn-type rocks (Fig. 1C). The main body of the Lar igneous complex includes grey to dark grey volcanic rocks such as lava and pyroclastic breccias which were intruded by non-mineralised and mineralised plutonic rocks such as stocks and dykes (Figs 1C, 2A–B). Re-Os dating of two molybdenite samples from two different drill holes has yielded ages of 29.72 ± 0.11 and 31.95 ± 0.11 Ma, suggesting that the mineralisation system was active for at least 2.2 myr (Boomeri et al., 2019) and showing that all above-mentioned igneous rocks are older than 32 Ma. Structurally, there are at least two fault and fracture systems in the Lar igneous complex (Fig. 1C). The first is the main fault system with a NW–SE trend, parallel to the Zahedan fault. The second fault system with a NE–SW trend is younger than the first one.

3. Material and methods

In the present study, mapping was done by using numerous field survey and satellite images for harsh areas; in addition, sampling was done on the basis of variety, texture and mineralogy of igneous rocks and in consideration of standard conditions. A total of 200 samples were collected from different rock types and standard thin sections were made. Thin sections were studied using a polarised microscope for petrographical and mineralogical descriptions at the University of Sistan and Baluchestan in Iran.

Major, trace and rare elements were determined by LiBO_2 fusion and measured by XRF techniques, and trace elements, including 14 rare earth elements, were obtained by LiBO_2 fusion and measured by ICP-MS techniques at the ACTLABS laboratory in Canada. The selected samples include K-rich intermediate intrusions ($n = 6$), K-rich intermediate dykes ($n = 3$) and K-rich intermediate volcanic rocks ($n = 6$) (Table 2).

4. Petrography

4.1. Volcanic rocks

The volcanic rocks are mainly grey and green in colour and porphyritic in texture with at least 50 per cent phenocrysts and occur as lava and pyroclastic rocks. As far as composition is concerned, they include andesites, trachyandesites, latites, trachytes, pyroclastics, leucites, dacites and basalts (Table 1).

4.1.1. Andesites

Andesites are porphyritic in texture. Plagioclase is the most abundant phenocryst, being euhedral with zoning and polysynthetic twinning, and 0.5–2 mm in size, partially broken and sericitised. Clinopyroxene is euhedral to subhedral and variable in size. Amphibole is subhedral, green to brown in colour and strongly pleochroic. It is rarely found in the groundmass, but is usually observed as a phenocryst. In addition, where the amount of K-feldspar increases, the rock can be referred to as trachyandesite.

4.1.2. Latites

Latites with porphyritic and cataclastic textures have a compositional range of latite, latite-trachyte, latite-andesite and quartz-bearing latite-andesite. Quartz amounts to 5 per cent in the quartz-bearing latite-andesite. K-feldspar (sanidine) and plagioclase are subhedral, 0.4–1 mm in size and are partially altered to sericite. Plagioclase has zoning and polysynthetic twinning. Sanidine is characterised by only Carlsbad twinning. Biotite is subhedral to anhedral, 0.4–1.5 mm in size, brown in colour and strongly pleochroic, being partially altered to chlorite.

4.1.3. Trachytes

Trachytes typically comprise trachyte and alkali-feldspar trachyte that show similar characteristics, even though the latter is richer in K-feldspar (Fig. 2C). These rocks are porphyritic to trachytic in

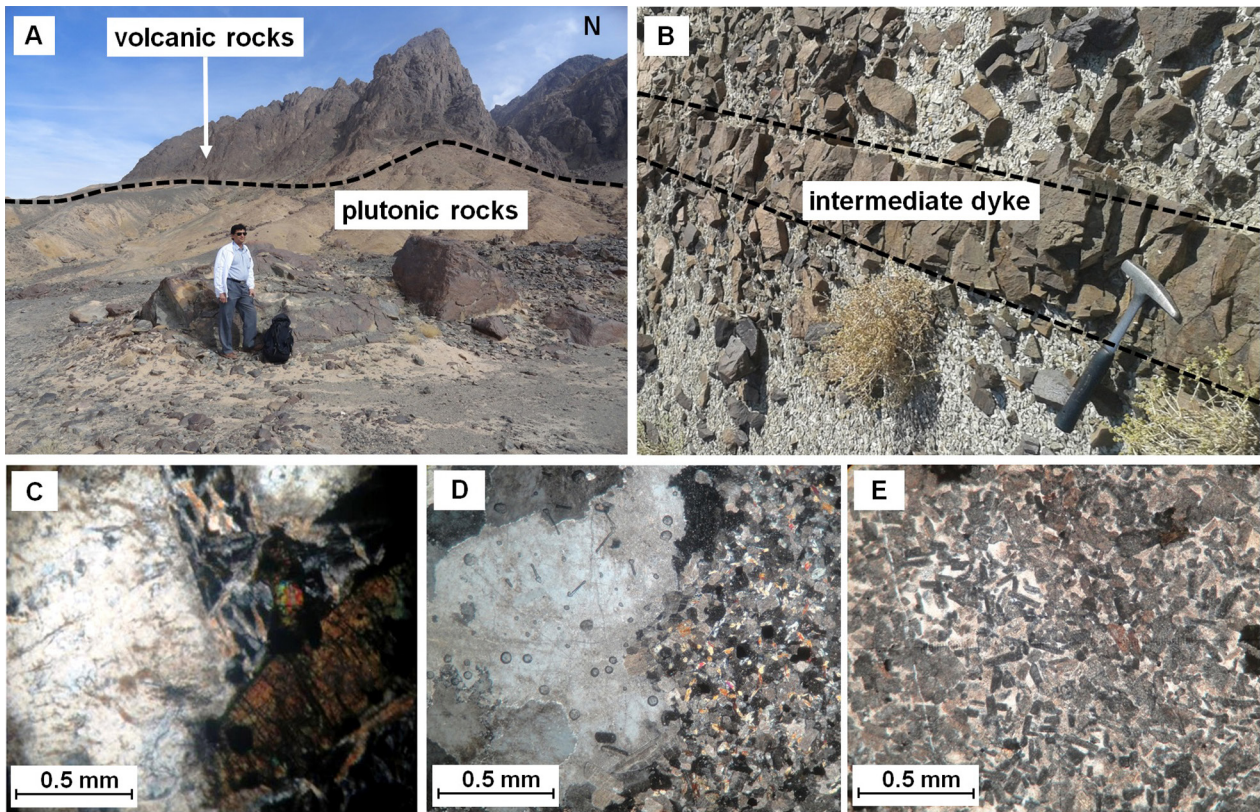


Fig. 2. Field photographs of: A -Volcanic and plutonic rocks; B -Intermediate dyke; cross-polarised light photomicrographs of: C - trachyte; D - porphyritic syenite; E - monzonite

texture. The phenocrysts of K-feldspar (sanidine), biotite, clinopyroxene and amphibole are embedded in a fine-grained groundmass of sanidine microlites. Sanidine is euhedral to subhedral, and variable in size (up to 5 mm) and partially altered to sericite and kaolinite. Biotite is euhedral, 0.3–0.7 mm in size, brownish green in colour and occasionally altered to chlorite. Clinopyroxene is euhedral to subhedral, 0.4–0.8 mm in size and green in colour. Amphibole is subhedral, 0.3–0.7 mm in size and also green in colour.

4.1.4. Pyroclastics

The pyroclastic rocks are typically composed of tuff, latite-tuff, andesite-tuff, trachyandesite-tuff and lithic-tuff. K-feldspar is subhedral and of variable size; in some cases it is altered to sericite and kaolinite. Plagioclase has a variable size and polysynthetic twinning. Clinopyroxene is subhedral and also variable in size. Amphibole is hornblende in composition, green in colour and variable in size. Biotite is from other ferro-magnesian minerals in pyroclastic rocks and occurs in three groups. The first group is rippling, brown in colour and variable in size. The second group occurs as assemblage rims around clinopyroxene and opaques and the third group

of biotite is finer than the other two, occurring and poikilitically in other minerals such as K-feldspar.

4.1.5. Leucitites

Leucitite is porphyritic in texture. The leucite phenocrysts are coarse grained (0.4–2 mm) and form pseudo-leucite when replaced by orthoclase and nepheline. Clinopyroxene is euhedral to subhedral, 0.3–2 mm in size with a green rim of amphibole and biotite.

4.1.6. Dacites

Dacite is predominantly porphyritic in texture. Plagioclase is subhedral to euhedral with polysynthetic twinning that in some cases is sericitised and hosts opaque veinlets. Biotite is thin, brown in colour and strongly pleochroic. Amphibole is subhedral, brown to green and partially altered to biotite. The quartz occurs as rounded phenocrysts and finer grains in the groundmass.

4.1.7. Basalts

Basalt is porphyritic in texture. Plagioclase is euhedral to subhedral, variable in size and partially altered to calcite and sericite. Clinopyroxene is euhedral to subhedral and variable in size.

4.2. Plutonic rocks

The plutonic rocks of the Lar igneous complex occur mainly as syenitic to monzonitic stocks and dykes (Table 1).

4.2.1. Syenites

Syenites are granular, porphyritic and occasionally cataclastic, poikilitic, micro-granular, equigranular and layered in texture (Fig. 2D). Based on variation in mineral content and textures, syenites typically have a range of alkali feldspar syenite, quartz alkali feldspar syenite, quartz syenite, leucosyenite, micro-syenite, micro-leucosyenite and Mela-syenite (shonkinite).

In petrographical studies, K-feldspar is mainly orthoclase and occasionally microcline in composition, tabular and subhedral to anhedral, variable in size (from 1 to up to 30 mm) and poikilitic, perthitic and microperthitic in texture. Perthites show a patchy intergrowth of orthoclase and albite. Some of the K-feldspar phenocrysts poikilitically contain inclusions of biotite, sphene, apatite, plagioclase, pyroxene and opaques. In some cases, the poikilitic texture was formed at the margin of K-feldspar.

K-feldspar is occasionally altered to sericite or clay minerals and sometimes has veinlets of secondary minerals. Plagioclase is tabular to lath and euhedral to subhedral, 0.5–2 mm in size, with oscillatory zoning and polysynthetic twinning that in some cases has a rim of orthoclase or is altered to sericite.

Clinopyroxene is subhedral to euhedral, 0.3–0.8 mm in size and partially to totally replaced by secondary amphibole, biotite, chlorite and epidote. Clinopyroxene is subhedral to euhedral, 0.2–4 mm in size, light green in colour, poikilitic in texture and occasionally has twinning which is partially altered. Amphibole is subhedral to euhedral, 0.6 mm in size, green in colour, strongly pleochroic; in some cases it has a rim of ilmenite. The primary biotites are subhedral to euhedral and occasionally bent, 0.3–4 mm in size, light to dark brown in colour, strongly pleochroic and with inclusions of apatite, sphene and opaques. Some biotites are formed around Fe-Ti oxides, amphibole and clinopyroxene. Finer biotites are found as inclusions in other minerals such as feldspars. Olivine is subhedral, >0.4 mm in size and strong in interferences, showing numerous fractures. Olivine shows a reaction rim of mica.

Table 1. Mineralogy of Lar igneous complex rocks

| Rocks | Volcanic | | | | | Plutonic | | | |
|------------|------------------|--------------------|-------------------------|---|-------------------|---------------|------------------------|---|-------------------------|
| | Andesites | Latites | Trachytes | Pyroclastics | Leucitites | Dacites | Basalts | Syenites | Monzonites |
| Mineralogy | Pl = 30% | Pl = 20% | Kfs = 30% | Kfs, Pl, Bt, Cpx, Amp, Ap, Ep, Qz, Ser, Kln, lithic fragments | Lct/Psl = 30% | Pl = 30–40% | Pl = 30% | Kfs = 70% | Kfs = 49% |
| | Amp = 40–50% | Kfs = 20% | Pl = 10% | | Cpx, Amp = 15–25% | Kfs = 5% | Cpx = 20% | Pl = 25% | Pl = 39% |
| | Ap, Bt, Opq = 5% | Bt, Cpx, Opq = 10% | Bt, Cpx, Amp = 10% | | Iron oxides ≅ 40% | Qz = 4–10% | ±Ol, Lct, Ep, Opq, Ser | Qz ≤ 5% | Qz ≤ 5% |
| | | ±Chl | ±Ap, Opq, Ser, Kln, Chl | | ±Ap, Opq, Bt | Bt = 2–10% | | ±Cpx, Ol, Amp, Bt, Spn, Ap, Zrn, sporadic Qz, Ep, Cal, Kln, Chl, Ser, Opq | Bt, Cpx, Amp = 10% |
| | | | | | | Amp = 2–5% | | | ±Spn, Ap, Opq, Chl, Ser |
| | | | | | | ±Ap, Opq, Ser | | | |

Pl - Plagioclase; Amp - Amphibole; Ap - Apatite; Bt - Biotite; Opq - Opaque mineral; Kfs - K-feldspar; Cpx - Clinopyroxene; Lct - Leucite; Psl - Pseudo-leucite; Qz - Quartz; Ol - Olivine; Ep - Epidote; Spn - Sphene; Zrn - Zircon; Cal - Calcite; Kln - Kaolinite; Chl - Chlorite; Ser - Sericite.

Apatite is almost prismatic and 0.4–0.8 mm in size, whereas finer apatite occurs as inclusions in other minerals. Sphene is subhedral to euhedral, 0.2–0.4 mm in size and high in relief. The igneous opaques are mainly magnetite, ilmenite and rutile, while hydrothermal opaques are mainly sulphide minerals such as pyrite, chalcopyrite, molybdenite and bornite.

4.2.2. Monzonites

Monzonitic rocks are typically composed of monzonite and quartz monzonite. In general, syenite and monzonite show similar characteristics, even though the latter has higher proportions of plagioclase and is grey in colour. The monzonitic rocks are granular, porphyritic and occasionally cataclastic in texture (Fig. 2E). Quartz monzonite has higher proportions of quartz, while K-feldspar and plagioclase occur in approximately equal amounts. Porphyritic monzonite is more heterogeneous and silicified. K-feldspar is orthoclase in composition, subhedral to anhedral, variable in size and poikilitic and perthitic in texture. K-feldspar poikilitically encloses plagioclase, biotite, sphene and opaques. Plagioclase is subhedral to euhedral, variable in size, poikilitic in texture with polysynthetic twinning and zoning that is occasionally altered to sericite.

The primary biotite is subhedral to euhedral, 0.4–4 mm in size, light to dark brown in colour and occasionally altered to chlorite. These biotites have poikilitic inclusions of plagioclase, sphene, apatite and opaques. Some biotites are finer in size and lighter in colour, having formed around and inside clinopyroxene, amphibole and opaques, and also occur in fractures. Clinopyroxene is subhedral to

euhedral, 0.2–0.7 mm in size and replaced by chlorite. Amphibole is subhedral to euhedral, 0.2–0.7 mm in size, green in colour, strongly pleochroic that is occasionally replaced by biotite and chlorite. The monzonite hosts veins and veinlets of malachite, iron oxides, sulphide minerals, quartz and phyllosilicates.

5. Whole rock geochemistry

5.1. Chemical classification

According to the geochemical classifications of Middlemost (1985) and Pearce (1996), the Lar plutonic rocks are monzonite, syenite and foid syenite and the volcanic rocks are alkalibasalt, andesite, basaltic andesite, trachyte and trachyandesite (Fig. 3).

5.2. Major and trace element chemistry

The whole rock major and trace elements content of representative igneous rocks is presented in Table 2, and some of these are plotted in Harker diagrams *vs* SiO₂ (Fig. 4). In Harker diagrams, the contents of Al₂O₃, CaO and MgO are highly variable in intermediate rocks. The contents of K₂O, P₂O₅ and Fe₂O₃, V and Sr decrease with increasing SiO₂. Leucitite has lower SiO₂ and higher K₂O and P₂O₅, whereas trachytes have higher SiO₂ and Al₂O₃. SiO₂ contents in intermediate K-rich dykes are higher than in intermediate K-rich stocks.

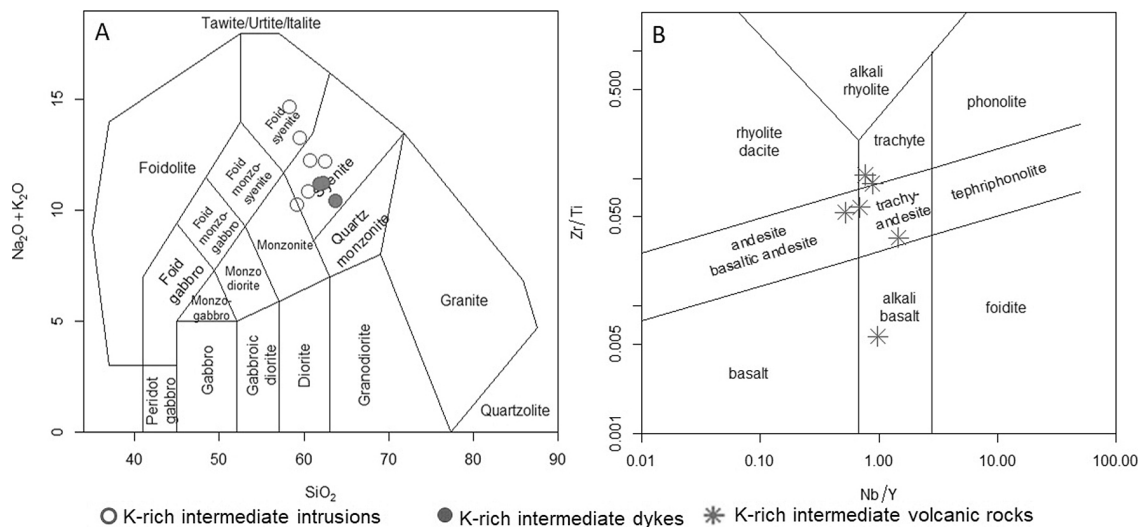


Fig. 3. Geochemical plots of the Lar igneous complex rocks in: A - Total alkali *vs.* silica (Middlemost, 1985); B - Nb/Y *vs.* Zr/Ti (modified from Pearce, 1996)

The Lar igneous complex chondrite-normalised REE patterns are characterised by an enrichment of LREE relative to HREE (Fig. 5A). The ratio of LREE/HREE is high in the Lar igneous complex rocks. Intermediate K-rich intrusions, intermediate K-rich volcanic rocks and intermediate K-rich dykes have slightly steep slopes in LREEs, mild slopes in MREEs and constant slopes in HREEs (Table 2; Fig. 5A).

A small, yet significant Eu anomaly, or none at all, is apparent in intermediate K-rich intrusions, intermediate K-rich volcanic rocks and intermediate K-rich dykes ($Eu/Eu^* = 0.72-1.10$, $0.73-0.91$, $0.70-0.85$). Although the intermediate samples con-

tain high amounts of K-feldspar and plagioclase, which usually have positive Eu anomalies (Taylor & McLennan, 1985), these might have been compensated by relatively high contents of minerals with negative Eu anomalies, such as amphibole.

The Lar igneous complex N-MORB-normalised multi-elements diagrams are characterised mostly by an enrichment in K, Rb, Th and a depletion of Ti, Zr, Hf, Y and Yb (Fig. 5B). These features are common in arc settings and are ascribed mostly to subduction enrichment and fluid metasomatism processes in subduction zones (Pearce et al., 1995) and/or can be explained by the retention of these elements in the residual mantle source during partial

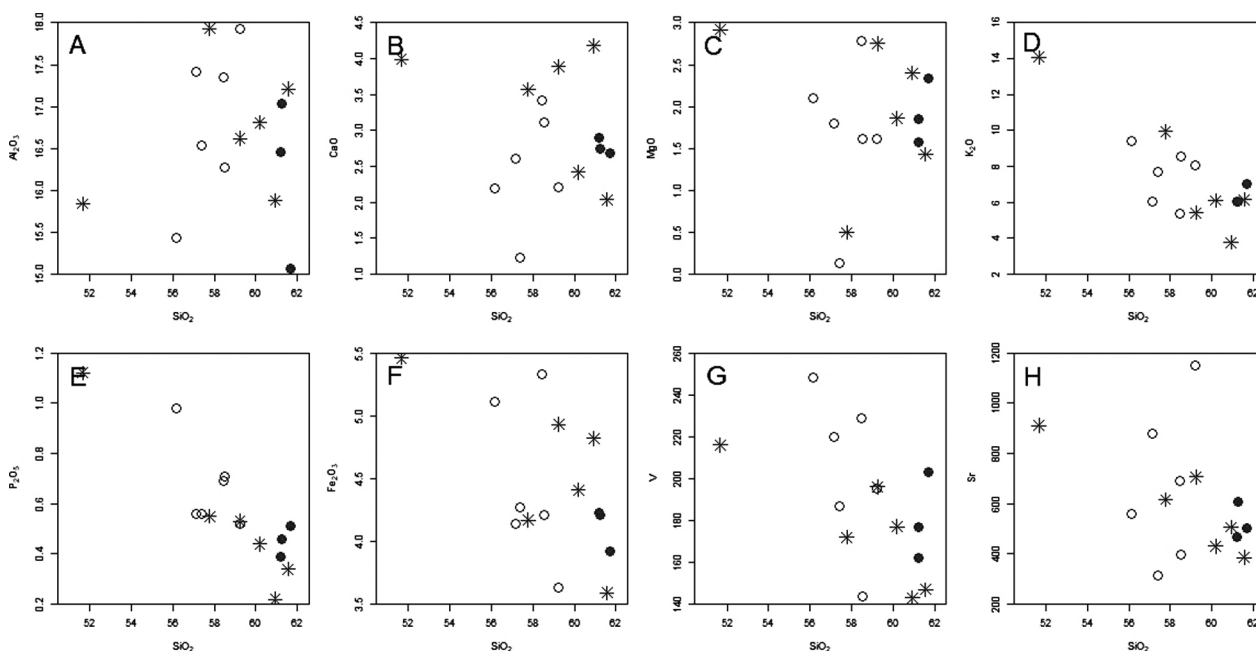


Fig. 4. Selected Harker variation diagrams of major (wt. %) and trace (ppm) elements vs. SiO_2 (wt. %) for the Lar igneous complex rocks. Graphic signs the same as in Fig. 3

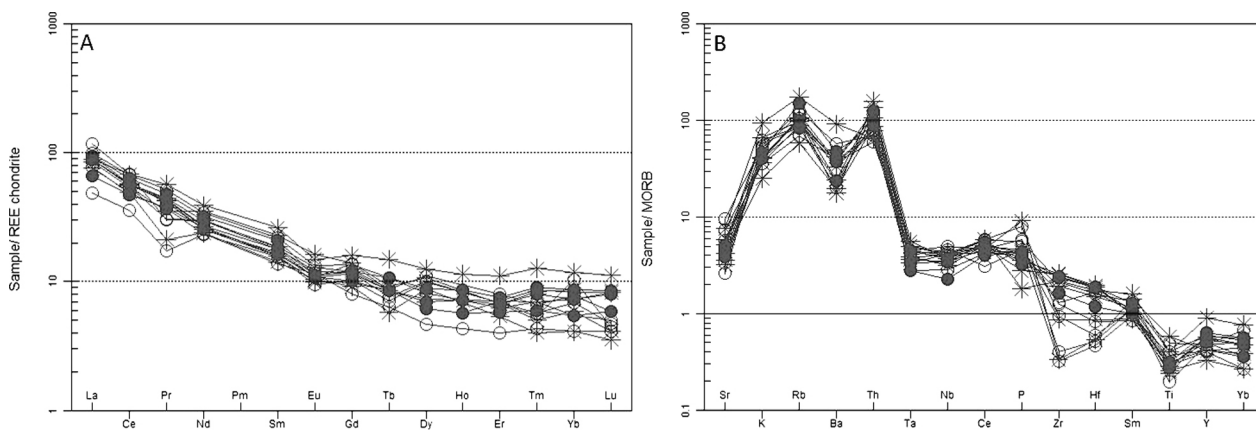


Fig. 5. A - Chondrite-normalised REE patterns (Nakamura, 1974); B - MORB-normalised REE patterns (Pearce, 1983) of the Lar igneous complex rocks. Graphic signs the same as in Fig. 3

Table 2. Representative major (wt. %) and trace (ppm) element analyses of the Lar igneous complex K-rich intermediate rocks

| Rocks | Plutonic | | | | | | | | | | | | | | |
|------------------------------------|----------|-------|--------|-------|------------|-------|-------|-------|-------|-------|-------|-------|-------|-------|--------|
| | Dykes | | | | Intrusions | | | | | | | | | | |
| | Volcanic | | | | | | | | | | | | | | |
| SiO ₂ | 61.24 | 61.69 | 61.20 | 59.22 | 58.45 | 58.52 | 56.15 | 57.39 | 57.14 | 51.66 | 60.19 | 59.24 | 57.77 | 61.56 | 60.93 |
| Al ₂ O ₃ | 17.03 | 15.07 | 16.46 | 17.93 | 17.35 | 16.28 | 15.44 | 16.54 | 17.42 | 15.84 | 16.81 | 16.62 | 17.93 | 17.21 | 15.88 |
| Fe ₂ O ₃ | 4.21 | 3.92 | 4.23 | 3.63 | 5.33 | 4.21 | 5.11 | 4.27 | 4.14 | 5.46 | 4.41 | 4.93 | 4.17 | 3.59 | 4.82 |
| MnO | 0.04 | 0.04 | 0.07 | 0.04 | 0.08 | 0.04 | 0.02 | 0.03 | 0.08 | 0.06 | 0.05 | 0.09 | 0.04 | 0.05 | 0.08 |
| MgO | 1.85 | 2.34 | 1.57 | 1.61 | 2.78 | 1.62 | 2.10 | 1.13 | 1.80 | 2.92 | 1.86 | 2.75 | <1 | 1.43 | 2.40 |
| CaO | 2.74 | 2.69 | 2.90 | 2.21 | 3.42 | 3.12 | 2.19 | 2.23 | 2.61 | 3.99 | 2.42 | 3.89 | 3.57 | 2.04 | 4.18 |
| Na ₂ O | 5.08 | 3.10 | 5.01 | 3.92 | 4.78 | 4.51 | 4.73 | 4.52 | 4.20 | 2.28 | 5.07 | 4.51 | 3.27 | 5.04 | 6.13 |
| K ₂ O | 6.02 | 7.01 | 6.05 | 8.05 | 5.37 | 8.55 | 9.43 | 7.71 | 7.04 | 14.08 | 6.11 | 5.42 | 9.94 | 6.16 | 3.77 |
| TiO ₂ | 0.41 | 0.44 | 0.47 | 0.43 | 0.60 | 0.74 | 0.29 | 0.55 | 0.47 | 0.87 | 0.43 | 0.49 | 0.38 | 0.36 | 0.61 |
| P ₂ O ₅ | 0.46 | 0.51 | 0.39 | 0.52 | 0.69 | 0.71 | 0.98 | 0.56 | 0.56 | 1.12 | 0.44 | 0.53 | 0.55 | 0.34 | 0.22 |
| LOI | 0.79 | 2.91 | 2.11 | 1.37 | 1.72 | 1.66 | 1.90 | 2.70 | 2.71 | 1.61 | 0.99 | 0.75 | 2.34 | 0.83 | 1.39 |
| Total | 99.87 | 99.71 | 100.46 | 98.93 | 100.57 | 99.96 | 98.34 | 97.63 | 98.17 | 99.89 | 98.78 | 99.23 | 99.96 | 98.61 | 100.41 |
| Sc | 8 | 10 | 9 | 5 | 11 | 6.7 | 10.4 | 8 | 6 | 9.2 | 8 | 11 | 4.7 | 7 | 13 |
| V | 177 | 203 | 162 | 195 | 229 | 144 | 248 | 187 | 220 | 216 | 177 | 196 | 172 | 147 | 143 |
| Ba | 749 | 954 | 476 | 1152 | 794 | 400 | 744 | 757 | 740 | 1836 | 485 | 849 | 663 | 355 | 396 |
| Sr | 608 | 501 | 468 | 1151 | 689 | 398.2 | 557.3 | 314.3 | 878 | 911.2 | 431 | 706 | 616.3 | 386 | 507 |
| Y | 17 | 15 | 19 | 12 | 18 | 14.2 | 14.2 | 12.4 | 12.6 | 12.2 | 17 | 16 | 9.8 | 17 | 27 |
| Zr | 211 | 147 | 218 | 112 | 192 | 36 | 85 | 29 | 117 | 30 | 232 | 174 | 78 | 230 | 197 |
| Cr | 30 | 30 | 40 | 40 | 30 | 21 | 32 | 32 | 40 | 111 | 30 | 110 | 22 | 20 | 90 |
| Co | 9 | 11 | 9 | 9 | 13 | 8.2 | 10.2 | 5.9 | 11 | 14.2 | 10 | 13 | 6.1 | 7 | 11 |
| Ni | 20 | 20 | 30 | 20 | 30 | 15 | 18 | 12 | 30 | 70 | 20 | 30 | 12 | 20 | 40 |
| Rb | 201 | 304 | 167 | 253 | 138 | 170 | 173 | 232 | 210 | 351 | 210 | 176 | 197 | 213 | 117 |
| Nb | 13 | 8 | 12 | 10 | 14 | 17.2 | 14.6 | 16.1 | 14 | 11.9 | 15 | 11 | 14.3 | 13 | 14 |
| La | 29.5 | 22 | 31.4 | 25.5 | 32.9 | 28 | 39 | 16 | 31 | 28 | 29.4 | 29.1 | 25 | 29.3 | 29.3 |
| Ce | 49.7 | 40.5 | 55 | 42.1 | 57.8 | 47 | 59 | 31 | 50 | 47 | 48.6 | 50.2 | 43 | 49.2 | 58.8 |
| Pr | 4.86 | 4.17 | 5.38 | 4.15 | 5.84 | 3.42 | 3.38 | 1.93 | 4.6 | 3.93 | 4.79 | 4.98 | 2.37 | 4.75 | 6.38 |
| Nd | 17.1 | 16.5 | 20.2 | 14.8 | 21.6 | 19 | 18.7 | 14.7 | 16 | 22 | 16.8 | 18.6 | 15 | 16 | 24.6 |
| Sm | 3.6 | 3.3 | 4.2 | 2.8 | 4.4 | 3.75 | 3.61 | 3.14 | 3.4 | 4.64 | 3.2 | 3.8 | 2.89 | 3.2 | 5.3 |
| Eu | 0.82 | 0.84 | 0.85 | 0.89 | 1.02 | 0.86 | 0.93 | 0.73 | 0.84 | 1.25 | 0.76 | 0.99 | 0.8 | 0.78 | 1.14 |
| Gd | 3.2 | 2.8 | 3.3 | 2.2 | 3.7 | 3.39 | 3.18 | 2.84 | 3.8 | 3.84 | 2.8 | 3.3 | 2.53 | 2.7 | 4.4 |
| Tb | 0.4 | 0.4 | 0.5 | 0.3 | 0.5 | 0.41 | 0.36 | 0.33 | 0.4 | 0.43 | 0.4 | 0.4 | 0.27 | 0.4 | 0.7 |
| Dy | 2.4 | 2.1 | 3 | 1.6 | 2.8 | 3.77 | 3.47 | 3.41 | 2.1 | 3.65 | 2.5 | 2.5 | 3.01 | 2.4 | 4.3 |
| Ho | 0.5 | 0.4 | 0.6 | 0.3 | 0.5 | - | - | - | 0.4 | - | 0.5 | 0.5 | - | 0.5 | 0.8 |
| Er | 1.5 | 1.3 | 1.7 | 0.9 | 1.6 | 1.81 | 1.54 | 1.53 | 1.6 | 1.52 | 1.4 | 1.5 | 1.21 | 1.5 | 2.5 |
| Tm | 0.24 | 0.18 | 0.27 | 0.13 | 0.26 | 0.2 | 0.16 | 0.17 | 0.21 | 0.15 | 0.21 | 0.24 | 0.12 | 0.25 | 0.38 |
| Yb | 1.6 | 1.2 | 1.9 | 0.9 | 1.8 | 1.7 | 2.3 | 1.5 | 1.2 | 1.3 | 1.6 | 1.6 | 0.9 | 1.9 | 2.6 |
| Lu | 0.27 | 0.2 | 0.29 | 0.14 | 0.28 | 0.2 | 0.15 | 0.16 | 0.17 | 0.14 | 0.28 | 0.28 | 0.12 | 0.29 | 0.38 |
| Hf | 4.4 | 2.8 | 4.5 | 2 | 3.8 | 1.24 | 1.43 | 1.11 | 4 | 1.28 | 4.5 | 3.6 | 2.08 | 4.7 | 4.2 |
| Ta | 0.8 | 0.5 | 0.6 | 0.5 | 0.8 | 0.8 | 0.67 | 0.72 | 0.8 | 0.65 | 0.9 | 0.7 | 0.6 | 1 | 0.9 |
| Pb | 21 | 9 | 19 | 27 | 16 | 18 | 19 | 18 | 24 | 30 | 9 | 58 | 37 | 17 | 10 |
| Th | 25.3 | 17.7 | 19.2 | 14.1 | 21.6 | 24.69 | 14.68 | 15.62 | 12 | 13.01 | 27.3 | 21.3 | 15.53 | 31.6 | 17.4 |
| U | 6.2 | 6 | 5.8 | 4.7 | 5.4 | 5.8 | 4.1 | 3.9 | 3.8 | 4 | 7.7 | 7.2 | 4.4 | 9 | 5.1 |
| Eu/Eu* | 0.74 | 0.85 | 0.70 | 1.10 | 0.78 | 0.74 | 0.84 | 0.75 | 0.72 | 0.91 | 0.78 | 0.86 | 0.91 | 0.82 | 0.73 |
| Ba/Rb | 3.73 | 3.14 | 2.85 | 4.55 | 5.75 | 2.35 | 4.30 | 3.26 | 3.52 | 5.23 | 2.31 | 4.82 | 3.37 | 1.67 | 3.38 |
| Rb/Sr | 0.33 | 0.61 | 0.36 | 0.22 | 0.20 | 0.43 | 0.31 | 0.74 | 0.24 | 0.39 | 0.49 | 0.25 | 0.32 | 0.55 | 0.23 |
| Sr/Y | 35.76 | 33.40 | 24.63 | 95.92 | 38.28 | 28.04 | 39.25 | 25.35 | 69.68 | 74.69 | 25.35 | 44.13 | 62.89 | 22.71 | 18.78 |
| Zr/Y | 12.41 | 9.80 | 11.47 | 9.33 | 10.67 | 2.54 | 5.99 | 2.34 | 9.29 | 2.46 | 13.65 | 10.88 | 7.96 | 13.53 | 7.30 |
| K ₂ O/Na ₂ O | 1.19 | 2.26 | 1.21 | 2.05 | 1.12 | 1.90 | 1.99 | 1.71 | 1.68 | 6.18 | 1.21 | 1.20 | 3.04 | 1.22 | 0.62 |
| Nb/Y | 0.76 | 0.53 | 0.63 | 0.83 | 0.78 | 1.21 | 1.03 | 1.30 | 1.11 | 0.98 | 0.88 | 0.69 | 1.46 | 0.76 | 0.52 |
| Nb/Th | 0.51 | 0.45 | 0.63 | 0.71 | 0.65 | 0.70 | 0.99 | 1.03 | 1.17 | 0.91 | 0.55 | 0.52 | 0.92 | 0.41 | 0.80 |
| Nb/U | 2.10 | 1.33 | 2.07 | 2.13 | 2.59 | 2.97 | 3.56 | 4.13 | 3.68 | 2.98 | 1.95 | 1.53 | 3.25 | 1.44 | 2.75 |
| Nb/La | 0.44 | 0.36 | 0.38 | 0.39 | 0.43 | 0.61 | 0.37 | 1.01 | 0.45 | 0.43 | 0.51 | 0.38 | 0.57 | 0.44 | 0.48 |
| La/Nb | 2.27 | 2.75 | 2.62 | 2.55 | 2.35 | 1.63 | 2.67 | 0.99 | 2.21 | 2.35 | 1.96 | 2.65 | 1.75 | 2.25 | 2.09 |
| La/Ta | 36.88 | 44.00 | 52.33 | 51.00 | 41.13 | 35.00 | 58.21 | 22.22 | 38.75 | 43.08 | 32.67 | 41.57 | 41.67 | 29.30 | 32.56 |

melting (Pearce, 1982; Wilson, 1989). In addition, these depletion and enrichment trends with respect to MORB may also be explained as reflecting melt generation from a source that is depleted by previous extraction and then enriched in subduction-mobile incompatible trace elements (Ali, 2012). Finally, the geochemical signatures mentioned may be attributed to involvement of fluids that were transported into the mantle wedge from the subduction slab (Leeman et al., 1990; Baker, 1994; Grove et al., 2002). However, variable partial melting rates of the MORB source mantle can play a major role where the above-mentioned geochemical signatures are concerned (Hughes, 1990).

The strong negative Ti anomaly (Fig. 5B) may be due to the early crystallisation and fractionation of Fe-Ti oxides, which buffers Ti concentration or caused earlier removal of Fe-Ti phases such as ilmenite and titanomagnetite (Obeid, 2006; Ozgenc & Ilbeyli, 2009). In addition, this anomaly can also be due to retention of Ti in rutile (Ali, 2012). On the other hand, some elements like P show variable trends in the Lar igneous complex rocks due to changes in apatite content (Fig. 5).

6. Discussion

6.1. Magmatic series

Based on geochemical studies by Camp & Griffis (1982), the Lar igneous complex is mainly alkaline. Other studies have asserted that the igneous rocks in this complex were linked to alkaline-ultrapotassic magmatism (e.g., Farokh-Nezhad, 2011), ultrapotassic magmatism (Ghafari-Bijar, 2009) and alkaline-potassic-ultrapotassic magmatism (Soltanian, 2013). In contrast to previous studies in which the Lar igneous complex was introduced mainly as alkaline in the magmatic series, the present study shows that Lar samples are mainly shoshonitic and high-K calc-alkaline (Fig. 6A, B). The Lar igneous complex rocks mainly have high values of K (>2 wt. per cent) that are in accordance with shoshonitic rocks. The potassic character of the igneous rocks in the Lar igneous complex area could also be proved by K_2O values that exceed those of Na_2O (Table 2), which classify them mainly as shoshonitic (Fig. 6A). In the diagram proposed by Liégeois et al. (1998), the Lar igneous complex igneous rocks plot

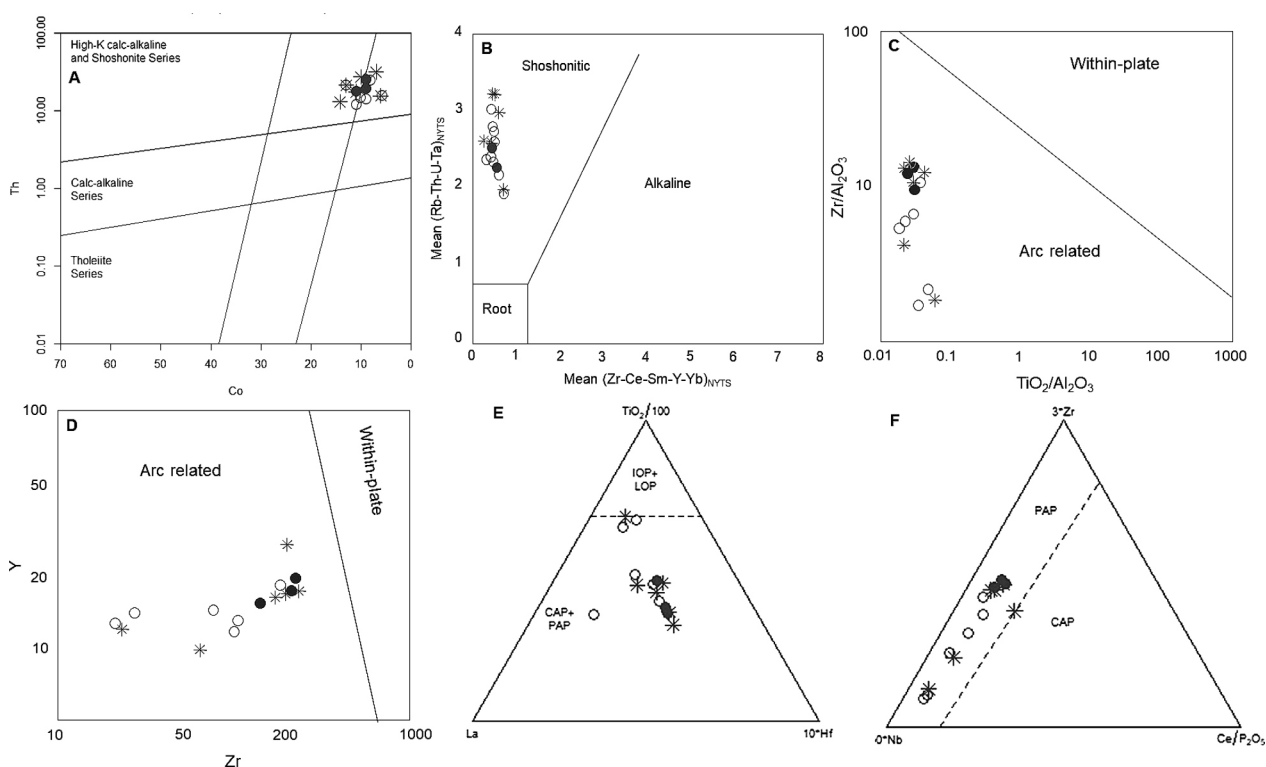


Fig. 6. Compositional characteristics of the Lar igneous complex rocks in various discrimination diagrams. **A** – Plot of Co vs. Th (Hastie et al., 2007); **B** – Sliding normalisation diagram for shoshonitic and alkaline rocks (Liégeois et al., 1998). Tectonic discrimination diagrams for potassic rocks (Müller et al., 1992) of: **C** – TiO_2/Al_2O_3 vs. Zr/Al_2O_3 ; **D** – Zr vs. Y; **E** – La-TiO₂-Hf; **F** – $Nb*50-Zr*3-Ce/P_2O_5$. IOP = Initial oceanic arc potassic rocks, LOP = Late oceanic arc potassic rocks, CAP = Continental arc potassic rocks, PAP = Post-collisional arc potassic rocks. Graphic signs the same as in Fig. 3

in the shoshonitic field, characterised by high SNY (= mean $[\text{Rb-U-Th-Ta}]_{\text{NYTS}}$) values and low SNX (= mean $[\text{Zr-Ce-Sm-Y-Yb}]_{\text{NYTS}}$) values (Fig. 6B).

6.2. Geotectonic environment

Shoshonitic igneous rocks occur in a wide range of tectonic settings such as continental arcs, oceanic arcs, post-collisional settings and within-plate settings (Müller et al., 1992). The Lar igneous complex rocks have high concentrations of LILE, intermediate LREE and low HFSE (Table 2). These geochemical features are more closely similar to rocks that are associated with arc-related settings. Tectonic discrimination diagrams (Fig. 6C, D) also show that the Lar igneous complex rocks are arc related. In oceanic island arcs (initial oceanic arcs and late oceanic arcs) potassic igneous rocks generally have the lowest concentrations of LILE, LREE and HFSE (e.g., potassic igneous rocks derived in initial oceanic arcs have <42 ppm La, <33 ppm Ce). In contrast, the continental and post-collisional potassic igneous rocks are enriched in Zr, Hf, Nb and LREE; they also have higher Sr and Ba contents, higher K/Na, Nb/Y (>0.55) and higher LREE/HREE ratios than potassic igneous rocks of oceanic arcs (Müller & Groves, 2016). Tectonic discrimination diagrams also show that the Lar igneous complex rocks fall within the post-collisional field (Fig. 6E, F). According to Camp & Griffis (1982), the age of the Lar igneous complex is younger than the time of collision (33 Ma) of the Afghan and Lut blocks in the south-eastern part of Iran and indicates a post-collisional tectonic setting for the Lar igneous complex magmatism. Barbarin (1999) and Bonin (2004) believed that the high-K calc alkaline granitoids could also have formed in passing from the compressional to tensional regimes and could be classified into the post-collisional groups of granitoids. The Lar igneous complex formed at the edge of the Zahedan strike-slip fault that has a length of 150 kilometres.

6.3. Source characteristics

There is a general consensus that potassic magmas cannot be derived by partial melting of normal mantle peridotite and instead require heterogeneous mantle sources that are metasomatically enriched in LILE and LREE (Edgar, 1987; Foley & Peccerillo, 1992; Guo et al., 2013; Kuritani et al., 2013; Tan et al., 2013; Bucholz et al., 2014; Aghazadeh et al., 2015; Yang et al., 2015). In general, K-rich magmatism in a post-collisional tectonic setting is generated mainly

from enriched mantle sources and/or metasomatised lithospheric mantle and includes shoshonitic lavas, lamprophyres and K-rich granitoids (Bonin et al., 1998; Vaughan & Sacrow, 2003; Seifert, 2008).

Following Sun and McDonough (1989), the Zr/Y ratio can separate depleted and enriched sources as higher Zr/Y values (>2.46) are typical of an enriched source, which is the case for the Lar igneous complex rocks that show an average Zr/Y of 8.64. Furthermore, it is suggested that potassic rocks with high K₂O, Th and Sr/Y, and low Cr, Ni, Y, MgO and HREE contents can be generated from partial melting of thickened lower crust and lithosphere (Chung et al., 2003; Hou et al., 2004; Hu et al., 2017; Zhang et al., 2017).

On the other hand, high contents of K₂O in the rocks studied require potassic phases (K-feldspars or phlogopite) in the source rocks. A weak or absent Eu anomaly, showing positive correlation with Sr, indicates that source magma fractionation was driven by feldspars, under relatively reduced conditions, enabling feldspars to be a sink for Eu. Furman & Graham (1999) indicated that melts produced from phlogopite had Rb/Sr > 0.1 and Ba/Rb < 15, while those formed from an amphibole-bearing source had Rb/Sr < 0.06 and Ba/Rb > 15. Rb/Sr ratios of the rocks studied range from 0.2 to 0.74 and their Ba/Rb ratios are less than 15. Based on these ratios it can be suggested that amphibole is also a rare phase in the source. Therefore, the main phase of the source rocks was phlogopite.

N-MORB-normalised multi-element diagrams of the Lar igneous complex rocks show a LREE(s) and LILE enrichment relative to HREE and HFSE, respectively, and Nb and Ti negative anomalies that point to involvement of a subduction-related environment that likely was inherited from a mantle source that had been metasomatised by melts/fluids released from a subducting slab, or modified by subducted sediments and associated fluids/melts (Foley et al., 1987; Altherr et al., 2008; Boari et al., 2009) (Fig. 5). Dehydration of a subducted slab could produce and release complex fluids to metasomatise the upper mantle wedge (lithospheric mantle wedge) (Tatsumi et al., 1986; Peacock, 1993; Arculus, 1994). Hydration and metasomatism of the mantle wedge lowered the mantle solidus temperature to the point at which melting begins (Tatsumi et al., 1986; Peacock, 1993; Arculus, 1994). Strike-slip faults can channel mantle materials and also generate deep-lithospheric heat. They can create a space for deep-seated magmas that make their way upwards along strike-slip faults, as a result of decompression melting (Pirajno, 2010). The product of such source melting (phlogopite-rich source) is a K-rich melt. This melt is distin-

guished from MORB by its higher H_2O , LILE and lower Ti, Nb and Ta contents, because certain high field strength elements, such as Ti, Nb, Hf, Y and Yb, are not mobilised by this metasomatic process and remain in source rocks of the slab, while large ion lithophile elements (LILE), such as K, Cs and Ba, are mobilised in the melt produced (Tatsumi et al., 1986; Peacock, 1993; Arculus, 1994). As mentioned earlier, the Lar igneous complex is related to a post-collisional tectonic setting and the behaviour of the trace elements mentioned indicates incorporation of subduction-related materials from previous subduction in the mantle source region. Moreover, these characteristics have also been reported for magmas that are derived from partial melting of a metasomatised mantle in a post-collisional setting (Jiang et al., 2012; Yang et al., 2012; Pang et al., 2013).

6.4. Evolutionary processes of magmatism in the Lar igneous complex

According to Glenn (2004) the #mg, Ni, Cr, and SiO_2 in primary magma are >0.7 , 1,400 to 1,500ppm,

$<1,000$ ppm, and <50 per cent, respectively. The representative samples of the Lar igneous complex rocks show Ni, Cr and SiO_2 ranges from 12 to 70ppm, 20 to 111ppm and 51.66 to 61.69wt. per cent, respectively. The values mentioned demonstrate that the Lar igneous complex did not directly form from a primary mantle magma.

Figures 7A and B show strong positive correlations between U-Th and Ba- Ba/Yb which indicate the importance of fractional crystallisation in most of the Lar igneous complex rocks. On the other hand, according to Sun & McDonough (1989), Nb/Th, Nb/U and Nb/La in the primary mantle are 8.4, 34 and 1.04, respectively. The Lar igneous complex rocks have an average of 0.73, 2.56 and 0.48 for Nb/Th, Nb/U and Nb/La, respectively, i.e., values that are lower than those of the primary mantle and in accordance with crustal contamination. The ratios of $La/Nb > 1.5$ and $La/Ta > 22$ also indicate the role of crustal contamination in magmatic evaluation (Hart et al., 1989); in the Lar igneous complex these rocks are 2.22 and 40.02, respectively. The process mentioned can also be seen in Figures 7C and D.

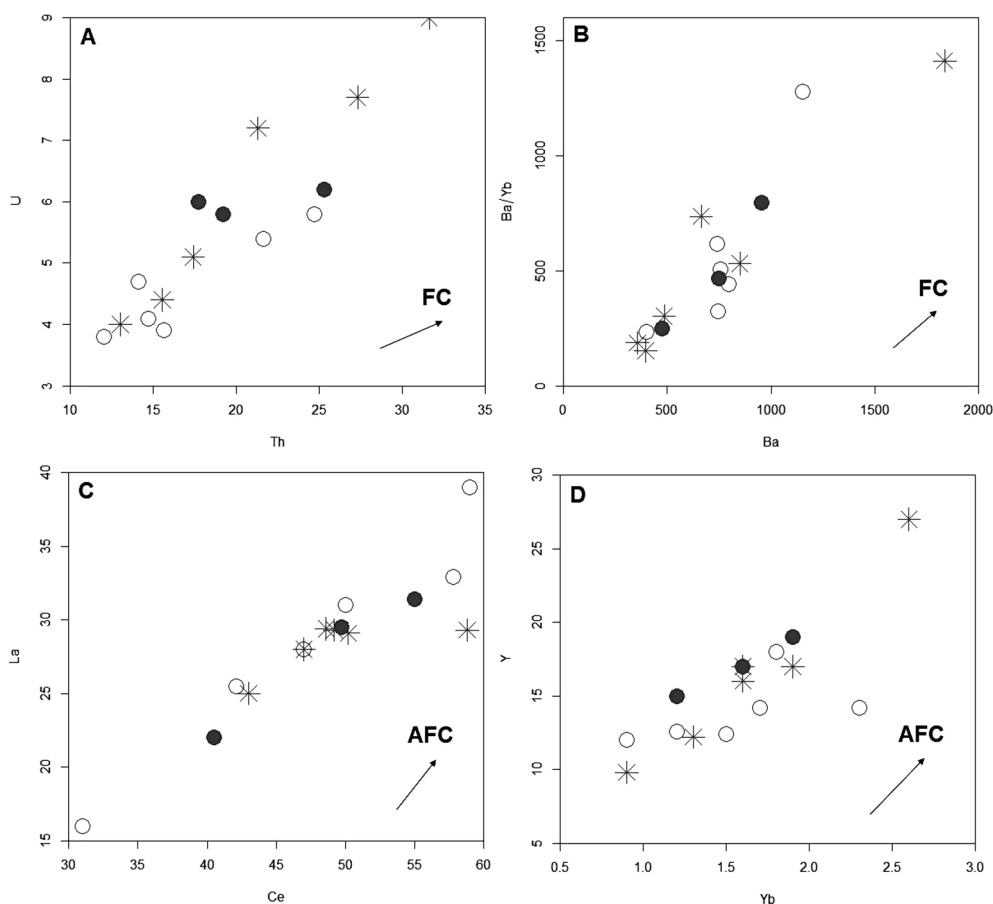


Fig. 7. Plots of: **A** - Th vs. U (Rollinson, 1993); **B** - Ba vs. Ba/Yb (Rollinson, 1993); **C** - Ce vs. La; **D** - Yb vs. Y. FC = fractional crystallisation, AFC = assimilation-fractional crystallisation. Graphic signs the same as in Fig. 3

7. Conclusions

Paleocene to Eocene flysch-type rocks were intruded by the Lar igneous complex about 32 myr ago. The Lar igneous complex rocks are classified into several types as follows: 1) intermediate K-rich volcanic rocks with a compositional range of trachyte, latite and andesite, 2) intermediate K-rich stocks and dykes with syenitic to monzonitic composition.

The Lar igneous complex rocks are K-rich, mainly shoshonitic in the magmatic series and derived from a post-collisional tectonic setting. They are characterised by an enrichment of LREE relative to HREE and LILE relative to HFSE, negative anomalies of Ti, Ba and Nb and positive anomalies of Rb and Th.

The K-rich shoshonitic igneous rocks were likely formed from magmas that were derived mainly from partial melting of a phlogopite-rich enriched lithospheric mantle. The arc-like geochemical signature of igneous rocks was probably inherited from an enriched mantle source that had been metasomatised by melts/fluids released from a subducting slab, or modified by subducted sediments and associated fluids/melts during a previous subduction process.

The intermediate plutonic and volcanic shoshonitic rocks probably crystallised from an similar, with a small degree of fractionation magma. This magma probably formed as a result of high-rate partial melting of a K-rich source.

Some of the Lar igneous complex rocks display high K_2O , Th and Sr/Y ratios with low Y and HREE contents, implying that they were derived from partial melting of thickened lithosphere.

References

- Aghazadeh, M., Prelevic, D., Badrzadeh, Z., Braschi, E., van den Bogaard, P. & Conticelli, S., 2015. Geochemistry Sr-Nd-Pb isotopes and geochronology of amphibole and mica-bearing lamprophyres in northwestern Iran: implications for mantle wedge heterogeneity in a paleo-subduction zone. *Lithos* 217, 352-369.
- Ali, S.A., 2012. *Geochemistry and geochronology of Tethyan-arc related igneous rocks, NE Iraq*. University of Wollongong, Australia, 363 pp.
- Altherr, R., Topuz, G., Siebel, W., Sen, C., Meyer, H.P., Satir, M. & Lahaye, Y., 2008. Geochemical and Sr-Nd-Pb isotopic characteristics of Paleocene plagioclitites from the Eastern Pontides (NE Turkey). *Lithos* 105, 149-161.
- Arculus, R.J., 1994. Aspects of magma genesis in arcs. *Lithos* 33, 189-208.
- Bagheri, S. & Bakhshi, M.R., 2001. *Investigation of north Zahedan magmatism and its relation to ore genesis*. University of Sistan and Baluchestan, Iran, 120 pp. (in Persian).
- Baker, M.B., Groves, T.L. & Price, R., 1994. Primitive basalts and andesites from the Mt. Shasta region, N. California: products of varying melt fraction and water content. *Contributions to Mineralogy and Petrology* 118, 111-129.
- Barbarin, B., 1999. A review of the relationships between granitoid types, their origins and their geodynamic environments. *Lithos* 46, 605-626.
- Boari, E., Tommasini, S., Laurenzi, M.A. & Conticelli, S., 2009. Transition from ultrapotassic kamafugitic to sub-alkaline magmas: Sr, Nd, and Pb isotope, trace element and Ar⁴⁰-Ar³⁹ age data from the middle Latin valley volcanic field, Roman magmatic province, central Italy. *Journal of Petrology* 50, 1327-1357.
- Bonin, B., 2004. Do coeval mafic and felsic magmas in post-collisional to within plate regimes necessarily imply two contrasting, mantle and crustal sources? A Review. *Lithos* 78, 1-24.
- Bonin, B.L., Azzouni-Sekkal, A., Bussy, F. & Ferrag, S., 1998. Alkali-calcic and alkaline post-orogenic (PO) granite magmatism: petrologic constraints and geodynamic settings. *Lithos* 45, 45-70.
- Boomeri, M., Lashkaripour, G.R. & Gorgij, M.N., 2005. F and Cl in biotites from Zahedan granitic rocks. *Iranian Journal of Crystallography and Mineralogy* 13, 79-94.
- Boomeri, M., Moradi, R., Stein, H. & Bagheri, S., 2019. Geology, Re-Os age, S and O isotopic composition of the Lar porphyry Cu-Mo deposit, southeast Iran. *Ore Geology Reviews* 104, 477-494.
- Bucholz, C.E., Jagoutz, O., Schmidt, M.W. & Sambuu, O., 2014. Fractional crystallization of high-K arc magmas: biotite- versus amphibole-dominated fractionation series in the Dariv Igneous Complex, western Mongolia. *Contributions to Mineralogy and Petrology* 168, 1072-1100.
- Camp, V.E. & Griffis, R.J., 1982. Character, genesis and tectonic setting of igneous rocks in the Sistan Suture Zone, eastern Iran. *Lithos* 15, 221-239.
- Chance, P., 1981. *Petrogenesis of a low-Ti, potassic suite: Kuh-e Lar caldera subsidence complex, eastern Iran*. University of Western Ontario, Canada.
- Chung, S.L., Liu, D., Ji, J., Chu, M.F., Lee, H.Y., Wen, D.J., Lo, C.H., Lee, T.Y., Qian, Q. & Zhang, Q., 2003. Adakites from continental collision zones: melting of thickened lower crust beneath southern Tibet. *Geology* 31, 1021-1024.
- Edgar, A.D., 1987. The genesis of alkaline magmas with emphasis on their source regions: inferences from experimental studies. [In:] J.G. Fitton & B.G.J. Upton (Eds): *Alkaline Igneous Rocks. Geological Society Special Publication* 30, 29-52.
- Farhoudi, G. & Karig, D.E., 1977. Makran of Iran and Pakistan as an active arc system. *Journal of Geology* 5, 664-668.
- Farokh-Nezhad, M., 2011. *Geochemical characterization of potassic mafic rocks, monzonites and syenites from Lar complex, eastern Iran*. University of Sistan and Baluchestan, Iran, 272 pp. (in Persian).

- Foley, S.F. & Peccerillo, A., 1992. Potassic and ultrapotassic magmas and their origin. *Lithos* 28, 181–185.
- Foley, S.F., Venturelli, G., Green, D.H. & Toscani, L., 1987. The ultrapotassic rocks: Characteristics, Classification, and Constraints for petrogenetic models. *Earth Science Review* 24, 81–134.
- Furman, T., Graham, D., 1999. Erosion of lithospheric mantle beneath the East African Rift system: geochemical evidence from the Kilvu volcanic province. *Lithos* 48, 237–262.
- Ghafari-Bijar, S., 2009. Geochemistry of potassic mafic rocks in the Lar complex, north of Zahedan, east of Iran. University of Sistan and Baluchestan, Iran, 161 pp. (in Persian).
- Ghasemi, H., Sadeghian, M., Kord, M. & Khanalizadeh, A., 2010. The evolution mechanisms of Zahedan granitoidic batholith, southeast Iran. *Iranian Journal of Crystallography and Mineralogy* 17, 551–578.
- Glenn, A.G., 2004. The influence of melt structure on trace element partitioning near the Peridotite solidus. *Contributions to Mineralogy and Petrology* 147, 511–527.
- Grove, T., Parman, S., Bowring, S., Price, R. & Baker, M., 2002. The role of an H₂O-rich fluid component in the generation of primitive basaltic andesites and andesites from the Mt. Shasta region, N California. *Contribution to Mineralogy and Petrology* 142, 375–396.
- Guo, Z., Wilson, M., Zhang, M., Cheng, Z. & Zhang, L., 2013. Post-collisional, K-rich mafic magmatism in south Tibet: constraints on Indian slab-to-wedge transport processes and plateau uplift. *Contribution to Mineralogy and Petrology* 165, 1311–1340.
- Harker, A., 1909. *The Natural History of Igneous Rock*. Macmillan, New York, 384 pp.
- Hart, W.K., Woldegabriel, G., Walter, R.C. & Mertzman, S.A., 1989. Basaltic volcanism in Ethiopia: constraints on continental rifting and mantle interactions. *Journal of Geophysical Research-Solid Earth* 94, 7731–7748.
- Hastie, A., Kerr, A., Pearce, J. & Mitchell, S., 2007. Classification of altered volcanic island arc rocks using immobile trace elements: development of the Th-Co discrimination diagram. *Journal of Petrology* 48, 2341–2357.
- Hou, Z.Q., Gao, Y.F., Qu, X.M., Rui, Z.Y. & Mo, X.X., 2004. Origin of adakitic intrusives generated during mid-Miocene east-west extension in southern Tibet. *Earth and Planetary Science Letters* 220, 139–155.
- Hu, P.Y., Zhai, Q.G., Jahn, B.M., Wang, J., Li, C., Chung, S.L., Lee, H.Y. & Tang, S.H., 2017. Late Early Cretaceous magmatic rocks (118–113 Ma) in the middle segment of the Bangong-Nujiang suture zone, Tibetan Plateau: Evidence of lithospheric delamination. *Gondwana Research* 44, 116–138.
- Hughes, S.S., 1990. Mafic magmatism and associated Tectonism of the central High Cascade Range, Oregon. *Journal of Geological Research* 95, 19623–19638.
- Jiang, Y.H., Jin, G.D., Liao, S.Y., Zhou, Q. & Zhao, P., 2012. Petrogenesis and tectonic implications of ultrapotassic microgranitoid enclaves in Late Triassic arc granitoids, Qinling orogen, central China. *International Geology Review* 54, 208–226.
- Kuritani, T., Kimura, J., Ohtani, E., Miyamoto, H. & Furuyama, K., 2013. Transition zone origin of potassic basalts from Wudalianchi Volcano, northeast China. *Lithos* 156, 1–12.
- Leeman, W.P., Smith, D.R., Hildreth, W., Palacz, A. & Rogers, N., 1990. Compositional diversity of late Cenozoic basalts in a transect across the southern Washington Cascades: implications for subduction zone magmatism. *Journal of Geophysical Research* 95, 19561–19582.
- Liégeois, J.P., Navez, J., Hertogen, J. & Black, R., 1998. Contrasting origin of post-collisional high-K calc-alkaline and shoshonitic versus alkaline and peralkaline granitoids. The use of sliding normalization. *Lithos* 45, 1–28.
- Middlemost, E.A.K., 1985. Naming materials in the magma/igneous rock system. *Earth Science Reviews* 37, 215–224.
- Mohammadi, A., Burg, J.P., Bouilhol, P. & Ruh, J., 2016. U-Pb geochronology and geochemistry of Zahedan and Shah Kuh plutons, Southeast Iran: Implication for closure of the South Sistan Suture Zone. *Lithos* 248, 293–308.
- Moradi, R., Boomeri, M. & Bagheri, S., 2014. Petrography and geochemistry of intrusive rocks in the Shurchah antimony-bearing area Southeast of Zahedan. *Journal of Petrology (Isfahan University)* 5, 15–32.
- Müller, D. & Groves, D., 2016. Potassic igneous rocks and associated gold-copper mineralization. Springer, Berlin, 311 pp.
- Müller, D., Rock, N.M.S. Groves, D.I., 1992. Geochemical discrimination between shoshonitic and potassic volcanic rocks from different tectonic settings: a pilot study. *Mineralogy and Petrology* 46, 259–289.
- Nakamura, N., 1974. Determination of REE, Ba, Fe, Mg, Na and K in carbonaceous and ordinary chondrites. *Geochimica et Cosmochim Acta* 38, 757–775.
- Obeid, M., 2006. The Pan-African arc-related volcanism of the Wadi Hodein area, south Eastern Desert, Egypt: Petrological and geochemical constraints. *Journal of African Earth Sciences* 44, 383–395.
- Ozgenç, I. & Ilbeyli, N., 2009. Geochemical constraints on petrogenesis of Late Cretaceous alkaline magmatism in east-central Anatolia (Hasancelebi-Basören, Malatya), Turkey. *Mineralogy and Petrology* 95, 71–85.
- Pang, K.N., Chung, S.L., Zarrinkoub, M.H., Khatib, M.M., Mohammadi, S.S., Chiu, H.Y., Chu, C.H., Lee, H.Y. & Lo, C.H., 2013. Eocene-Oligocene post-collisional magmatism in the Lut-Sistan region, eastern Iran: Magma genesis and tectonic implications. *Lithos* 180–181, 234–251.
- Peacock, S.M., 1993. Large-scale hydration of the lithosphere over subducting slabs. *Chemical Geology* 108, 49–59.
- Pearce, J.A., 1982. Trace element characteristics of lavas from destructive plate boundaries. [In:] R.S. Thorpe (Ed.): *Andesites: Orogenic Andesites and Related Rocks*. John Wiley and Sons., New York, 528–548.
- Pearce, J.A., 1983. Role of the sub-continental lithosphere in magma genesis at active continental margins. [In:] C.J. Hawkesworth & M.J. Norry (Eds): *Continental*

- Basalt and Mantle xenoliths*. Shiva Publ., Nantwich, 230–249.
- Pearce, J., 1996. A user's guide to basalt discrimination diagrams. Trace element geochemistry of volcanic rocks: applications for massive sulphide exploration. *Geological Association of Canada* 12, 79–113.
- Pearce, J.A., Baker, P.E., Harvey, P.K. & Luff, I.W., 1995. Geochemical evidence for subduction fluxes, mantle melting and fractional crystallization beneath the south sandwich island arc. *Journal of Petrology* 36, 1073–1109.
- Pirajno, F., 2010. Intracontinental strike-slip faults, associated magmatism, mineral systems and mantle dynamics: examples from NW China and Altay-Sayan (Siberia). *Journal of Geodynamics* 50, 325–346.
- Rahnama-Rad, J., Sahebzadeh, B., & Mirhajizadeh, A.A., 2008. Weathering and weakness of Zahedan granitoids: a rock engineering point of view. *Applied Geology* 4, 247–257.
- Rollinson, H.R., 1993. *Using Geochemical Data: Evaluation, Presentation, Interpretation*. Longman, 352 pp.
- Sadeghian, M. & Valizadeh, M.V., 2007. Emplacement mechanism of Zahedan granitoidic pluton with the aid of AMS method. *Earth Sciences* 17, 126–143.
- Sadeghian, M., Bouchez, J.L., Ne de lec, A., Siqueira, R. & Valizadeh, M.V., 2005. The granite pluton of Zahedan (southeast of Iran): a petrological and magnetic fabric study of a syntectonic sill emplaced in a transtensional setting. *Asian Journal of Earth Science* 25, 301–327.
- Seifert, Th., 2008. *Metallogeny and Petrogenesis of Lamprophyres in the Mid-European Variscides*. Millpress/IOS Press, Amsterdam, 303 pp.
- Soltanian, A., 2013. *Petrogenesis of volcanic rocks from Lar complex, north of Zahedan, east of Iran*. University of Sistan and Baluchestan, Iran, 93 pp. (in Persian).
- Stöcklin, J., 1968. Structural history and tectonics of Iran, a review. *American Association of Petroleum Geologists Bulletin* 52, 1229–1258.
- Sun, S. & McDonough, W.F., 1989. Chemical and isotopic systematics of oceanic basalts: Implications for mantle composition and processes. *Geological Society London, Special Publications* 42, 313–345.
- Tan, J., Wei, J.H., Shi, W.J., Feng, B., Li, Y.J. & Fu, L.B., 2013. Origin of dyke swarms by mixing of metasomatized subcontinental lithospheric mantle-derived and lower crustal magmas in the Guocheng fault belt, Jiaodong Peninsula, North China Craton. *Geological Journal* 48, 516–530.
- Tatsumi, Y., Hamilton, D.L. & Nesbitt, R.W., 1986. Chemical characteristics of fluid phase released from a subducted lithosphere and origin of arc magmas: evidence from high-pressure experiments and natural rocks. *Journal of Volcanology and Geothermal Research* 29, 293–309.
- Taylor, S.R. & McLennan, S.M., 1985. *The Continental Crust: its Composition and Evolution*. Blackwell, 312 pp.
- Tirrul, R., Bell, L.R., Griffis, R.J. & Camp, V.E., 1983. The Sistan Suture Zone of Eastern Iran. *Geological Society of American Bulletin* 94, 134–150.
- Vaughan, A.P.M. & Sacrow, J.M., 2003. K-rich mantle metasomatism control of localization and initiation of lithospheric strike-slip faulting. *Terra Nova* 15, 163–169.
- Walker, R. & Jackson, J., 2004. Active tectonics and Late Cenozoic strain distribution in central and eastern Iran. *Tectonics* 23, 1–24.
- Wilson, M., 1989. *Igneous petrogenesis: a global tectonic approach*. Unwin Hyman Ltd., London, 466 pp.
- Yang, W.B., Niu, H.C., Shan, Q., Luo, Y., Sun, W.D., Li, C.Y., Li, N.B. & Yu, X.Y., 2012. Late Paleozoic calc-alkaline to shoshonitic magmatism and its geodynamic implications, Yuximolegai area, western Tianshan, Xinjiang. *Gondwana Research* 22, 325–340.
- Yang, Z.M., Lu, Y.J., Hou, Z.Q. & Chang, Z.S., 2015. High-Mg diorite from Qulong in Southern Tibet: implications for the genesis of adakite-like intrusions and associated porphyry Cu deposits in collisional orogens. *Journal of Petrology* 56, 227–254.
- Zhang, L., Zhang, H., Zhang, S., Xiong, Z., Luo, B., Yang, H., Pan, F., Zhou, X., Xu, W. & Guo, L., 2017. Lithospheric delamination in post-collisional setting: Evidence from intrusive magmatism from the North Qilian orogen to southern margin of the Alxa block, NW China. *Lithos* 288–289, 20–34.

Manuscript submitted 10 September 2019

Revision accepted 15 March 2020